COMMUNICATIONS IN INFORMATION AND SYSTEMS
Vol. 2, No. 2, pp. 121-146, December 2002

002

COMPUTING CONFORMAL STRUCTURES OF SURFACES*

XIANFENG GU† AND SHING-TUNG YAU‡

Abstract. This paper solves the problem of computing conformal structures of general 2-manifolds represented as triangular meshes. We approximate the De Rham cohomology by simplicial cohomology and represent the Laplace-Beltrami operator, the Hodge star operator by linear systems. A basis of holomorphic one-forms is constructed explicitly. We then obtain a period matrix by integrating holomorphic differentials along a homology basis. We also study the global conformal mappings between genus zero surfaces and spheres, and between general surfaces and planes. Our method of computing conformal structures can be applied to tackle fundamental problems in computer aid geometry design and computer graphics, such as geometry classification and identification, and surface global parametrization.

Keywords. Mesh, conformal structure, texture mapping, Holomorphic forms, harmonic forms, period matrix

1. Introduction.

This paper introduces a systematic way to compute conformal structures of general 2d surfaces, including computing holomorphic differentials, period matrices and conformal maps among surfaces. To the best of our knowledge, this is the first paper to give a set of practical algorithms to compute conformal structures for general closed meshes. This method has the potential to be generalized to work on meshes with boundaries and other representations of surfaces, such as implicit surfaces and level sets.

Computational conformal geometry is an active field in mathematical research. The following objects are equivalent to one another:

1. Compact Riemann surfaces;
2. Projective algebraic curves;
3. Jacobian varieties of compact Riemann surfaces.

Basically the goal for computational conformal geometry is to compute conversion among these different representations, and to compute conformal invariants and conformal mappings among surfaces.

In [1], [2] and [3], Riemann surfaces are represented as algebraic curves or D/G, where D is the hyperbolic space and G is a Fuchsian group acting in D. The homology bases are constructed as Mobius transformations, then the holomorphic differentials are found by using algebraic geometry techniques on algebraic curves. Finally the period matrices are computed explicitly by integrating holomorphic differentials on a homology basis.

*Invited paper. Received on November 26, 2002; accepted for publication on December 27, 2002. This research project is solely supported by Geometric Informatics Inc.

†Division of Engineering and Applied Science, Harvard University, Cambridge, MA. E-mail: gu@eecs.harvard.edu

‡Mathematics Department, Harvard University, Cambridge, MA. E-mail: yau@math.harvard.edu

In real applications, geometric surfaces are represented as meshes. It is rare to represent general surfaces as algebraic curves or quotient spaces. The above methods for abstract representation of Riemann surfaces can not be applied directly. In this paper, we assume the input data are general meshes and propose a systematic way to compute their conformal structures.

In [4] an algorithm is introduced to use circle packing to approximate conformal mappings between planar regions. For general surfaces, circle packing only considers topological structures but not geometric structures. It cannot find the conformal mapping from a surface to the plane. However, if the triangulation is equilateral for each face, then the circle packing result is conformal. But, in general, such triangulation is difficult to construct. Therefore, circle packing method is not appropriate for our purpose.

In computer graphics, surface parametrization has been studied by many researchers. Hoppe et al. [5] use local harmonic maps for surface simplification and editing. Haker et al. [6] develop an algorithm to conformally map a genus zero surface to a sphere by solving a linear system. In [6], the sphere is stereo-graphically projected to the complex plane implicitly. The stereo-graphic projection is nonlinear in nature, large errors are introduced in the neighborhood of the north pole by using a piecewise linear mapping to approximate it in practice.

In [7], Desbrun et al. use conformal mappings to define geometry maps, where they compute the conformal maps from a topological disk to the complex plane. An equivalent algorithm is developed by Maillot et al. [8], who use conformal mappings for the purpose of non-distorted texture-mapping. Their method is based on the Riemann-Cauchy equation. So far, although conformal mappings of genus zero surfaces have been studied, no one has tried to compute global conformal mappings for non-zero genus surfaces.

In this paper, we solve the problem of computing conformal structures of surfaces thoroughly. For genus zero surfaces, we introduce a new method to construct conformal mappings from them to spheres directly. This method avoids the stereo-graphic projection and is more stable and accurate. More importantly, this method can be generalized to compute conformal mappings between arbitrary two genus zero surfaces. For surfaces with non-zero genus, the computation is much more complicated. We give a set of general algorithms to compute their conformal structures, including holomorphic differentials, period matrices and conformal mappings.

A mapping between two surfaces is a *conformal map* if it just scales the first fundamental form (so it preserves angles) everywhere. If there exists a bijective conformal map between two surfaces and the inverse is also conformal, then we call these two surfaces *conformally equivalent*. The conformal automorphisms form a group. The invariants under the conformal transformation group are called *conformal structure*. Our goal is to compute these conformal structures. In terms of surface classification, conformally equivalent classes are finer than topologically equivalent classes and

coarser than isometric classes.

Geometric object classification and identification have been studied for years, but still remain an open problem. It is challenging to classify general surfaces accurately and efficiently. A good algorithm should satisfy the following requirements: the method is intrinsically dependent of geometry and independent of triangulation; the method is stable in the sense that perturbation of geometry changes the result continuously; the method should also be robust enough to tolerate different resolutions and boundaries; for database indexing, each class index should be small for storage and easy to compute.

Conformal mapping has many nice properties to make it suitable for classification problems. Conformal mapping only depends on the Riemann metric and is independent of triangulation. Conformal mapping is continuously dependent of Riemann metric, so it works well for different resolutions. Conformal invariants can be represented as a complex matrix, which can be easily stored and compared. We propose to use conformal structures to classify general surfaces. For each conformally equivalent class, we can define canonical parametrization for the purpose of comparison.

Geometry matching can be formulated to find an isometry between two surfaces. By computing conformal parametrization, the isometry can be obtained easily. For surfaces with close metrics, conformal parametrization can also give the best geometric matching results.

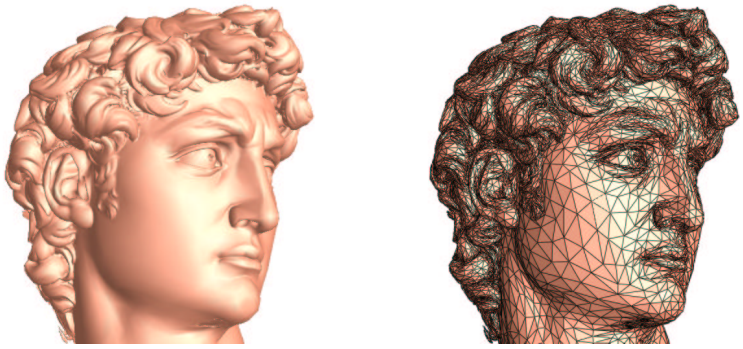

FIG. 1. *Surface & mesh with 20000 faces*

1.1. Preliminaries. In this section, we give a brief summary of concepts and notations.

Let K be a simplicial complex whose topological realization $|K|$ is homeomorphic to a compact 2-dimensional manifold. Suppose there is a piecewise linear embedding

$$F : |K| \to R^3. \tag{1}$$

The pair (K, F) is called a triangular mesh and we denote it as M. The q-cells of K

are denoted as $[v_0, v_1, \cdots, v_q]$. Figure 1 shows the surface of a King David sculpture and its mesh representation.

Because M has a simplicial complex structure, we can compute the simplicial homology $H_*(K, R)$ and cohomology $H^*(K, R)$. We denote the *chain complex* as $C_*K = \{C_qK, \partial_q\}_{q\geq 0}$, and *cochain complex* as $C^*K = \{C^qK, \delta^q\}_{q\geq 0}$, where $C^qK = Hom(C_qK; R)$. The boundary operator ∂_q and coboundary operator δ_{q+1} satisfy the following equation:

$$\delta^q \omega\sigma = \omega\partial_{q+1}\sigma, \tag{2}$$

where $\omega \in C^qK$ and $\sigma \in C_{q+1}K$. The kernel of ∂_q is Z_qK, the image of ∂_{q+1} is B_q, and the *q-th homology group* is

$$H_qK = Z_qK/B_qK. \tag{3}$$

Similarly, the kernel of δ^q is Z^qK, the image of δ^{q-1} is B^qK, and the *q-th cohomology group is*

$$H^q = Z^qK/B^qK. \tag{4}$$

The embedding F endows M with a differential structure. We then define the local charts of M as (T_i, ϕ_i),

$$\phi_i : T_i \to R^2, \tag{5}$$

where T_i is a face of M, and $\phi_i \circ F^{-1} : R^3 \to R^2$ is an isometry. Then M is a smooth manifold, we can compute the De Rham cohomology $H^*(\Omega(M; TM), d)$, where $\Omega(M; TM)$ is the set of *differential forms*, and d is the *exterior derivative*. In our setting, all computations are carried out on meshes, which are piecewise linear. Therefore, it is enough to just use piecewise linear differential forms on M. We define the set of piecewise linear forms as

$$\Omega^{PL}(M; TM) = \Omega_0^{PL} \cup \Omega_1^{PL} \cup \Omega_2^{PL}. \tag{6}$$

Here Ω_0^{PL} is the set of piecewise linear functions on M defined on its vertices. Ω_1^{PL} is the set of piecewise constant one-forms which are consistent along the edges,

$$\int_{[u,v]} \omega|_{[u,v,w]} = \int_{[u,v]} \omega|_{[t,v,u]}, \tag{7}$$

where $[u, v, w]$ and $[t, v, u]$ are the two faces adjacent to edge $[u, v]$. Ω_2^{PL} is the set of piecewise constant two-forms.

All the computations are defined for De Rham cohomology in concept and for simplicial cohomology in implementation. We connect differential forms with simplicial cocycles by the map $\Gamma : Z^qK \to \Omega_q^{PL}(M; TM)$: given $\omega \in Z^qK$, $\forall \sigma \in C_qK$,

$$\omega\sigma = \int_\sigma \Gamma\omega. \tag{8}$$

It is easy to verify that Γ is well defined, bijective and commutative to differential operators,

$$d \circ \Gamma = \Gamma \circ \delta. \tag{9}$$

So in the following discussion, we do not differentiate simplicial cocycles and piecewise linear differential forms explicitly.

1.2. Harmonic One-form and Holomorphic One-form. According to harmonic anylasis theories in [9], each cohomology class in $H(\Omega(M;TM),d)$ has a harmonic representative, which minimizes the harmonic energy as defined below. Suppose $f \in \Omega^0(M;TM)$, the harmonic energy of f is

$$E(f) = \frac{1}{2}\int_M ||df||^2 d\sigma. \tag{10}$$

The norm is Euclidean norm, $d\sigma$ is the area element. The harmonic energy for one-forms is defined similarly. Suppose $\omega \in \Omega^1(M;TM)$, the harmonic energy of ω is

$$E(\omega) = \frac{1}{2}\int_M ||\omega||^2 d\sigma. \tag{11}$$

In the case where M is a mesh, the harmonic energy can be simplified in the format of string energy and defined on C^*K. Suppose $f \in C^0K$, the harmonic energy 10 can be rewritten as

$$E(f) = \sum_{[u,v]\in K} k_{u,v}||f(u) - f(v)||^2. \tag{12}$$

For one-form $\omega \in C^1K$, the harmonic energy 11 is reformulated as

$$E(\omega) = \sum_{[u,v]\in K} k_{u,v}||\omega[u,v]||^2. \tag{13}$$

Suppose edge $[u,v]$ has two adjacent faces T_α, T_β, $T_\alpha = [v_0, v_1, v_2]$, define parameters

$$a^\alpha_{v_1,v_2} = \frac{1}{2}\frac{(v_1 - v_3)\cdot(v_2 - v_3)}{(v_1 - v_3)\times(v_2 - v_3)} \tag{14}$$

$$a^\alpha_{v_2,v_3} = \frac{1}{2}\frac{(v_2 - v_1)\cdot(v_3 - v_1)}{(v_2 - v_1)\times(v_3 - v_1)} \tag{15}$$

$$a^\alpha_{v_3,v_1} = \frac{1}{2}\frac{(v_3 - v_2)\cdot(v_1 - v_2)}{(v_3 - v_2)\times(v_1 - v_2)}. \tag{16}$$

(17)

$a^\beta_{u,v}$ can be defined similarly, then

$$k_{u,v} = a^\alpha_{u,v} + a^\beta_{u,v}. \tag{18}$$

A function $f \in C^0K$ with local minimum harmonic energy is called a *harmonic function*. A cocycle $\omega \in C^1K$ with local minimum harmonic energy is called a *harmonic one-form*.

The Laplacian operator $\Delta^{PL}: \Omega_0^{PL} \to \Omega_0^{PL}$ is defined as the derivative of $E(f)$ with respect to f,

$$\Delta^{PL} f|_u = \sum_{[u,v]\in K} k_{u,v}(f(u) - f(v)). \tag{19}$$

1.3. Complex Structure. A 2-dimensional manifold M has a natural complex structure. A complex structure is constructed explicitly in [10] for meshes.

Any genus zero surface M is conformally equivalent to S^2. A degree one map $\mathbf{u}: M \to S^2$ is conformal if and only if $\mathbf{u}$ is harmonic. The conformal automorphism group of S^2 is 6 dimensional, which is the *Mobius transformation group*. Map $\mathbf{u}$ can be uniquely determined by fixing three image points on S^2.

For a non-zero genus surface, we study the structure of its holomorphic differential group. The following form:

$$\omega + \sqrt{-1}\tau, \omega, \tau \in \Omega^1(M; TM) \tag{20}$$

is called a *holomorphic one-form* if both ω and τ are harmonic and τ is conjugate to ω, i.e. $*\omega = \tau$, where $*$ is the *Hodge star* operator. Suppose $\{v_1, v_2\}$ are orthonormal bases of a tangent space on M, then

$$\omega(v_1) = \tau(v_2),\ \omega(v_2) = -\tau(v_1). \tag{21}$$

The set of holomorphic one-forms is denoted as $H^{1,0}(M, \mathbb{C})$. Let M be a compact Riemann surface of genus g and $B = \{e_1, e_2, \cdots, e_{2g}\}$ be an arbitrary basis of $H_1(M, Z)$. The intersection matrix C of the above basis has entries

$$c_{ij} = -e_i \cdot e_j, \tag{22}$$

where the dot denotes the algebraic intersection number. A basis $B^* = \{\omega_1, \omega_2, \cdots, \omega_{2g}\}$ of the real vector space $H^{1,0}(M, \mathbb{C})$ is the dual of B if

$$Re \int_{e_i} \omega_j = c_{ij}. \tag{23}$$

From Riemann bilinear relations [11] it follows that the matrix S with entries

$$Im \int_{e_i} \omega_j = s_{ij} \tag{24}$$

is symmetric and positive definite. The complex structure in $H^{1,0}(M, \mathbb{C})$ is given by a matrix R with respect to the basis B^* and satisfies $R^2 = -I$. The following relation holds:

$$CR = S. \tag{25}$$

After Weyl [12] and Siegel [13], the matrix R is called the period matrix of M with respect to the basis B. Let a be a holomorphic automorphism of M, and let $[a]$ denote

the matrix of its action on the homology and cohomology with respect to the above basis, then

$$[a]^{-1}R[a] = R, [a]^T C[a] = C. \tag{26}$$

The pair (R, C) determines the conformal structure of a given Riemann surface in the following sense: two such pairs, (R_1, C_1) and (R_2, C_2) determine the same structure if and only if there exists an integral matrix N whose determinant is ± 1 such that

$$N^{-1}R_1N = R_2, N^T C_1 N = C_2. \tag{27}$$

If both B_1 and B_2 are canonic, then N is symplectic.

2. Conformal Mapping for Genus Zero Surfaces. Given two genus zero meshes M_1, M_2, there are many conformal mappings between them. All such conformal mappings form the Mobius transformation group. The algorithm for computing conformal mappings is based on the fact that degree one harmonic maps are conformal for genus zero surfaces. Our method is as follows: first find a homeomorphism $\mathbf{h}$ between M_1 and M_2, then diffuse $\mathbf{h}$ to be harmonic. In order to ensure the convergence of the algorithm, special constraints are added so that the solution is unique.

2.1. Constrained Variational Problem. Suppose M_1 and M_2 are genus zero meshes, $\mathbf{h} : M_1 \to M_2$ is a degree one mapping. We would like to minimize the harmonic energy $E(\mathbf{h})$,

$$E(\mathbf{h}) = \sum_{[u,v]\in K} k_{u,v}||\mathbf{h}(u) - \mathbf{h}(v)||^2, \mathbf{h} = (h_0, h_1, h_2). \tag{29}$$

The Laplacian for $\mathbf{h}$ is simply

$$\Delta^{PL}\mathbf{h} = (\Delta^{PL}h_0, \Delta^{PL}h_1, \Delta^{PL}h_2). \tag{30}$$

If $\mathbf{h}$ is harmonic, then the tangential component of $\Delta^{PL}\mathbf{h}$ is zero. Define the *projection operator*

$$P_{\mathbf{v}} = I - \frac{\mathbf{v}\otimes\mathbf{v}^T}{\mathbf{v}^T\mathbf{v}}, \mathbf{v} \in R^3, \tag{31}$$

where $\otimes$ is the tensor product and I is an identity matrix. Then $\mathbf{h}$ is harmonic if and only if

$$P_{\mathbf{n}\circ\mathbf{h}}\Delta^{PL}\mathbf{h} = 0, \tag{32}$$

where $\mathbf{n}$ is the normal on M_2.

In order to ensure that the process converges to a unique solution, we have to add extra constraints. We force the center of mass of the surface to be at the origin:

$$\int_{M_2} \mathbf{h} d\sigma_{M_1} = \mathbf{0}, \tag{33}$$

where $d\sigma_{M_1}$ is the area element on M_1. This constraint will guarantee the solution is unique up to a rotation. Then we can construct the partial differential equation

$$\frac{\partial \mathbf{h}}{\partial t} + P_{\mathbf{n}\circ\mathbf{h}}\Delta^{PL}\mathbf{h} = 0 \tag{34}$$

with constraints 33. The steady state solution of $\mathbf{h}$ is the conformal mapping from M_1 to M_2. Equation 34 can be solved by iterative methods efficiently.

2.2. Steepest Descendent Algorithm. In our implementation, we fix M_2 as S^2. In order to compute the initial homeomorphism from M_1 to S^2, we first compute the spherical barycentric embedding, which minimizes the barycentric string energy. In the string energy formulae 12, we let

$$k_{u,v} \equiv 1. \tag{35}$$

The corresponding Laplacian is defined as 19 with constant unit $k_{u,v}$. The following algorithm computes spherical barycentric embeddings.

Input A mesh M, step length δt, threshold ϵ.
Output A spherical barycentric mapping $\mathbf{h}$.

1. Compute the Gauss map $\mathbf{n}$ from M to S^2, $\mathbf{h} \leftarrow \mathbf{n}$.
2. Compute the barycentric energy $E(\mathbf{h})$, if $\delta E < \epsilon$ then return $\mathbf{h}$.
3. Compute the tangential Laplacian of $\mathbf{h}$, $\delta h \leftarrow P_{\mathbf{n}\circ\mathbf{h}}\Delta^{PL}\mathbf{h}$.
4. Update $\mathbf{h}$ by $\mathbf{h} \leftarrow \mathbf{h} - \delta t \times \delta\mathbf{h}$.
5. Repeat 2 through 4.

Algorithm 1. Spherical Barycentric Embedding

In practice, the barycentric embedding algorithm converges faster than the spherical harmonic embedding, and there are no extra constraints. Hence we use it as the initial embedding to compute spherical conformal mapping. The spherical conformal embedding algorithm is more complicated. In each iteration an extra normalization step is executed to force the mass center of the surface to stay in the origin during the entire process.

Gu-Yau Algorithm for genus zero meshes:
Input A mesh M, step length δt, threshold ϵ.
Output A spherical conformal mapping $\mathbf{h}$.

1. Compute the spherical barycentric map $\mathbf{b}$ from M to S^2, $\mathbf{h} \leftarrow \mathbf{b}$.
2. Compute the harmonic energy $E(\mathbf{h})$, if $\delta E < \epsilon$ then return $\mathbf{h}$.
3. Compute the tangential Laplacian of $\mathbf{h}$, $\delta\mathbf{h} \leftarrow P_{\mathbf{n}\circ\mathbf{h}}\Delta^{PL}\mathbf{h}$.
4. Update $\mathbf{h}$ by $\mathbf{h} \leftarrow \mathbf{h} - \delta t \times \delta\mathbf{h}$.

```
5.  Compute a Mobius transformation m, such that m ∘ h satisfies
    the center of mass constraint equation 33.
6.  Repeat 2 through 5.
```

Algorithm 2. Spherical Conformal Embedding

In step 5 above, the Mobius transformation $\mathbf{m}$ on S^2 is in the form $\phi^{-1} \circ f \circ \phi$, where ϕ is the stereo-graphic projection from S^2 to the complex plane,

$$\phi(x_0, x_1, x_2) = (\frac{x_0}{1+x_2}, \frac{x_1}{1+x_2}), (x_0, x_1, x_2) \in R^3, \tag{36}$$

f is a Mobius transformation on $\mathbb{C}$,

$$f(z) = \frac{az+b}{cz+d}, a, b, c, d \in \mathbb{C}, ad - bc \neq 0. \tag{37}$$

In practice, it is expensive to normalize $\mathbf{h}$ by Mobius transformations, we simply shift the center of mass of $\mathbf{h}(M_1)$ to the origin and normalize $\mathbf{h}(v), v \in K$ to the unit vector. The step length δt is chosen to be close to the square of the minimum edge length of M.

2.3. Results. The spherical barycentric embedding result is shown in figure 9. A mesh model of gargoyle with 20000 faces (a) is mapped to a sphere using algorithm 1 shown in (b). The normal information is preserved so the shading indicates the correspondence. During the optimization, the head and wing parts converge more slowly than the other regions. Special local optimization is performed for these parts.

Figure 9 (c) and (d) show the spherical conformal mapping and conformal texture-mapping. First, the gargoyle mesh is conformally mapped to a sphere. The upper and lower hemispheres are stereo-graphically projected to the tangent planes through its north pole and south pole individually. Then the gargoyle mesh is mapped to the 2 planes conformally. The texture-coordinates are defined as the plane coordinates and the texture is a regular checker board image. From snapshot (d), we can tell that the right angles at each corner are preserved.

Figure 10 shows the same process on a bunny mesh. Figure 10 (c) is the result of a Mobius transformation of (b) on a sphere.

We define the *streching factor* function as the scaling factor of the first fundamental forms. Suppose the first fundamental form of the mesh is ds^2, and (u, v) are the conformal coordinates (or texture coordinates in our case), then

$$ds^2 = \lambda(u, v)^2(du^2 + dv^2), \tag{38}$$

where $\lambda(u, v) : \mathbb{C} \to \mathbb{R}^+$ is the streching factor function.

The stretching factor is distributed non-uniformly. On the head, wings of the gargoyle and the ears of the bunny, stretching factors are relatively greater. This is indicated by the texture on those parts, where each pixel on texture covers more surface area. In general, any extruding parts have greater stretching factors.

Figure 11 shows the spherical conformal mapping of a brain mesh and its conformal texture-mapping.

Because conformal mapping is a local scaling of the first fundamental form, it preserves shapes locally. There is no distortion between the mesh and spherical image. By comparing figure 11 (a) and (b), one can find the correspondence of major geometric features easily.

3. Computing Conformal Structure for Non-zero Genus Meshes.

3.1. Overview. For non-zero genus meshes, the computation of conformal structure is much more complicated. The goal is to find a complete basis of the holomorphic one-form group. The algorithm can be summarized in the following steps:

Gu-Yau Algorithm `for non-zero genus meshes:`
Input `A mesh` M.
Output `A basis of holomorphic differentials` $\{\zeta_1 + \sqrt{-1}\,{}^*\zeta_1, \cdots, \zeta_{2g} + \sqrt{-1}\,{}^*\zeta_{2g}\}$.

1. `Compute a homology group basis` $B = \{e_1, e_2, \cdots, e_{2g}\}$.
2. `Compute the dual cohomology group basis` $\Omega = \{\omega_1, \omega_2, \cdots, \omega_{2g}\}$.
3. `Diffuse each` ω_i `to a harmonic one-form` ζ_i.
4. `Compute the conjugate of each` ζ_i`, denoted as` ${}^*\zeta_i$. `Construct holomorphic one-forms` $\zeta_i + \sqrt{-1}({}^*\zeta_i)$.

Algorithm 3. Compute Holomorphic Differentials

The following subsections explain each step in details.

3.2. Computing Homology. There are many methods for computing homology groups H_*K of a simplical complex K. In our implementation, we use the classic algorithm, which is based on reducing boundary operator matrices ∂_q's to their Smith normal forms [14]. In order to avoid the substantial computational cost of the reduction to the Simth normal forms, the mesh is simplified by using the progressive mesh algorithm introduced in [15]. Once the homology bases B are found on the coarse mesh, they are mapped back to the fine mesh through a sequence of vertex splits. At each vertex split step, we check the neighborhood of the current split vertex and preserve the connectivity of each homology base cycle in B. Finally, on the fine mesh, we use Dijkstra's algorithm to shorten each base cycle and perturb them to intersect transversely.

Figure 2 shows the homology bases of a torus mesh. The original mesh illustrated in (b) has 4000 faces and is simplified to 500 faces shown in (a). The base cycles are computed on the coarse mesh then lifted back to the original mesh. Figure 12 (a) shows a homology basis of a genus 2 mesh.

The fundamental domain is also computed by the retraction algorithm described

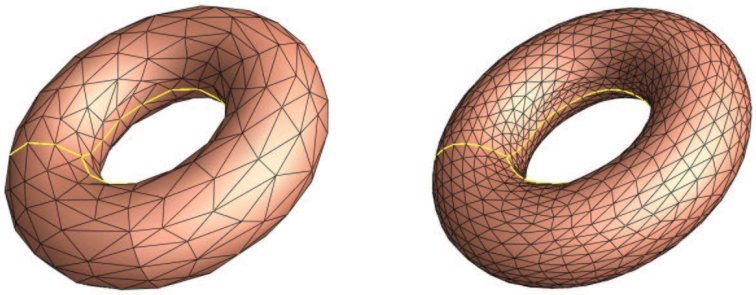

(a). 500 faces mesh (b). 4000 faces mesh

FIG. 2. *Homology bases for torus*

in [16]. The following is the basic procedure: at the beginning, we remove one arbitrary face and record the boundary. At each step we remove one face attached to the current boundary, all the removed faces always form a topological disk. The boundary of this disk is kept and updated until all faces are removed. Then we cut the mesh along the final boundary to get the fundamental domain. Figure 13 (d) shows a fundamental domain of the 2 hole torus mesh, (c) is the final boundary found by the retraction algorithm.

3.3. Computing Cohomology. Once we obtain a homology basis B, we can compute a cohomology basis Ω dual of B, such that

$$\int_{e_i} \omega_j = \delta_i^j, \tag{39}$$

where δ_i^j is the Kronecker symbol. We choose a handle and the pair of conjugate homology base cycles on it, denoted as $\{e_i, e_{i+g}\}$. Then we split the mesh along these 2 cycles, the boundary becomes $e_i e_{i+g} e_i^{-1} e_{i+g}^{-1}$. Next we map the entire mesh to a unit square, boundary to boundary, corner to corner. The interior mapping can be constructed by the Floater embedding algorithm as described in [17]. Then the one-forms $\{dx, dy\}$ are the duals of $\{e_i, e_{i+g}\}$.

Input A mesh M, a pair of conjugate base cycles $\{e_1, e_2\}$.
Output $\{\omega_1, \omega_2\} \in C^1 K$, which are dual to $\{e_1, e_2\}$.
1. Slice the mesh M open along $\{e_1, e_2\}$, $\partial M = e_1 e_2 e_1^{-1} e_2^{-1}$.
2. Map $e_1 e_2 e_1^{-1} e_2^{-1}$ to the boundary of $D = [0,1] \times [0,1]$ on $\mathbb{R}^2$.
3. Map the interior of M to D by Floater embedding method.
4. Return $\omega_1 \leftarrow dx$, $\omega_2 \leftarrow dy$.

Algorithm 4. Compute Cohomology

Figure 12 shows the computing process of a genus two mesh. Subfigure (a) illustrates the conjugate homology cycles. Then the mesh is sliced open along one pair of them, as shown in (b). The entire mesh is mapped to the unit square. The mapping is of degree one but not an immersion, as the second handle of the mesh is collapsed to the central region as shown in (c) and (d).

3.4. Computing Harmonic One-forms. Suppose a cohomology basis of mesh M is $\Omega = \{\omega_1, \omega_2, \cdots, \omega_{2g}\}$, we deform each ω_i to a harmonic one-form by adding an exact one-form δf_i, where $f_i \in C^0K$, such that $\omega_i + df_i$ minimizes the harmonic energy in equation 13.

Input A one-form $\tau \in C^1K$.
Output A harmonic one-form ω which is homologous to τ.

1. Define $F \in C^0K$, $F \leftarrow 0$.
2. Compute the Laplacian

$$\Delta^{PL}F|_u = \sum_{[u,v]\in K} k_{u,v}(F(u) - F(v) + \tau[u,v]). \tag{40}$$

3. $F \leftarrow F - \Delta^{PL}F \times \delta t$.
4. Compute the harmonic energy $E(\tau + \delta F)$. If $\delta E < \epsilon$ then $\omega \leftarrow \tau + \delta F$, ω.
5. Repeat 2 through 4.

Algorithm 5. Compute Harmonic One-forms

This is the most time-consuming step during the whole procedure. In practice, we perform local optimizations on those regions that converge more slowly.

3.5. Computing Holomorphic One-forms. Given a harmonic one-form basis $\Omega = \{\omega_1, \cdots, \omega_{2g}\}$, we can construct the bases of holomorphic one-forms directly by pairing ω_i with its conjugate ${}^*\omega_i$. Given $\omega \in C^1K$, then $\Gamma\omega \in \Omega_1^{PL}(M; TM)$. Suppose

$$\Gamma\omega = f dx + g dy, \tag{41}$$

where (x, y) are local coordinates as defined in equation 5, f, g are constants on each face of M. Then according to equation 21, ${}^*\Gamma\omega$ is formulated by:

$${}^*\Gamma\omega = f dy - g dx. \tag{42}$$

The Hodge star operator transforms harmonic one-forms to harmonic one-forms. If ω is harmonic, so is ${}^*\omega$. Hence ${}^*\omega$ can be represented as a linear combination of ω_i's. Suppose

$${}^*\omega = \sum_{i=1}^{2g} \alpha_i \omega_i. \tag{43}$$

Then we can compute the integration of wedge product

$$\int_M \omega_i \wedge {}^*\omega = \sum_{j=1}^{2g} \alpha_j \int_M \omega_i \wedge \omega_j = \int_M \Gamma\omega_j \wedge {}^*(\Gamma\omega), \tag{44}$$

where $i, j = 1, 2, \cdots, 2g$. Equation 44 can be formulated as the following linear system

$$\mathbf{W}\alpha = \mathbf{b}, \tag{45}$$

where $\alpha = (\alpha_1, \alpha_2, \ldots, \alpha_{2g})^T$, matrix $\mathbf{W}$ is with entries

$$w_{ij} = \int_M \omega_i \wedge \omega_j = \int_M \Gamma\omega_i \wedge \Gamma\omega_j. \tag{46}$$

Vector $\mathbf{b}$ has entries

$$b_i = \int_M \Gamma\omega_i \wedge {}^*(\Gamma\omega). \tag{47}$$

Assume $\Gamma\omega_i = f_i dx + g_i dy$, $\Gamma\omega = pdx + qdy$, from 42

$$w_{ij} = \sum_{[u,v,w]\in K} (f_i g_j - f_j g_i)\sigma_{[u,v,w]},\ b_i = \sum_{[u,v,w]\in K} (f_i p + g_i q)\sigma_{[u,v,w]}. \tag{48}$$

where $\sigma_{[u,v,w]}$ is the area of face $[u, v, w]$. By our construction, ω_i's are dual cocyles of e_i's, so $w_{ij} = e_i \cdot e_j$, matrix $\mathbf{W}$ equals the intersection matrix C of the current homology basis. Hence $\mathbf{W}$ is non-degenerated, ${}^*\omega$ exists and is unique. The following is the algorithm to compute holomorphic one-forms:

Input A harmonic 1-form basis $\{\omega_1, \omega_2, \cdots, \omega_{2g}\}$, a harmonic 1-form ω.
Output A holomorphic 1-form $\omega + \sqrt{-1}\,{}^*\omega$.

1. Compute $\Gamma\omega$ and $\Gamma\omega_i$'s.
2. Compute ${}^*\Gamma\omega$.
3. Compute the wedge products of $\int_M \omega_i \wedge \omega_j$ and $\int_M \omega_i \wedge {}^*\omega$.
4. Solve linear system 45, and get the conjugate of ω, ${}^*\omega$.
5. Let $\zeta \leftarrow \omega + \sqrt{-1}\,{}^*\omega$, return ζ.

Algorithm 6. Compute Holomorphic Forms

By applying the above algorithm, we can compute the bases of holomorphic differentials of M. Suppose we treat the holomorphic differentials as a complex vector space, we denote a basis as $\{\zeta_1, \zeta_2, \cdots, \zeta_g\}$, where g is the genus of M. Figure 13 shows the results of computing a holomorphic one-form basis of a genus two mesh. Figure 13 (a) is ζ_1, (b) is ζ_2, visualized by texture-mapping.

By linearly combining ζ_i's, we can construct all holomorphic one-forms on M. By integrating holomorphic one-forms on the fundamental domain, the mesh is globally conformally mapped to the plane with finite singularities. The number of singularities

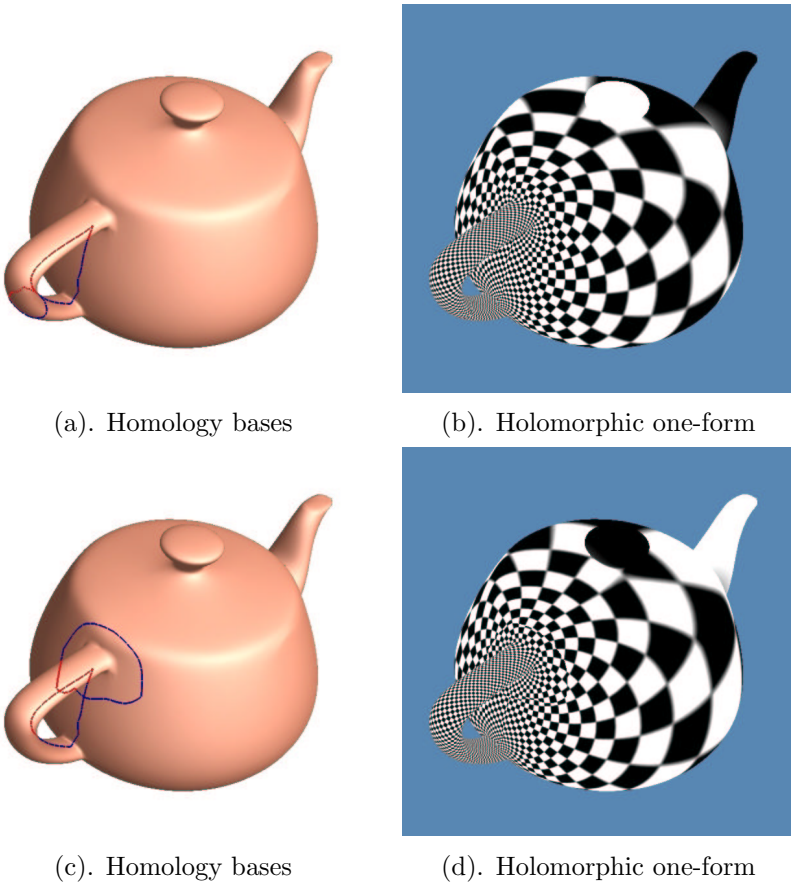

(a). Homology bases (b). Holomorphic one-form

(c). Homology bases (d). Holomorphic one-form

FIG. 3. *Boundary independent conformal mapping*

on M is $2g-2$. Figure 14 (a) shows $\zeta_1+\zeta_2$, figure 14(c) shows $\zeta_1-\zeta_2$. The singularities of $\zeta_1+\zeta_2$ are at the front and back sides of the torus. Those of $\zeta_1-\zeta_2$ are on the left and right sides.

Figure 14 (b) and (d) also show the level sets of stretching factors as defined in equation 38 on the mesh. These level sets have rich geometric information of mesh M.

4. Performance Analysis. The algorithm is independent of the choice of geometric realization of homology base cycles, but dependent of their homology classes. In a future paper, we will give a method to compute global conformal parametrization which is independent of the choice of homology classes. Figure 3 shows the result of holomorphic one-forms using different cuts. In figure 3 (a), there are two conjugate homology cycles represented as dark curves. In (c), one of them is deformed to a homologous one. (b) and (d) are the resulting holomorphic forms illustrated by texture-mapping. From these figures, we can see that the texture mapping patterns and the stretching factors are very similar. We can also see that conformality

is preserved everywhere, even across the cut boundaries.

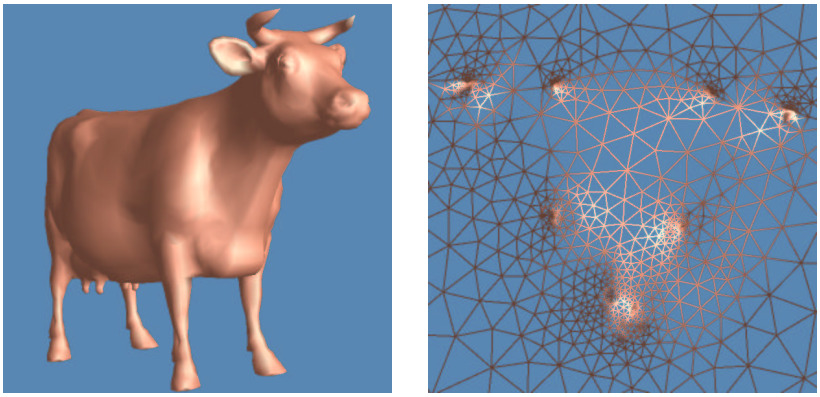

Cow mesh Embedding of the head region

FIG. 4. *Extruding regions*

Figure 4 shows the embedding of a cow head on the plane. It is obvious that the extruding parts, like the nose, ears and horns are mapped to relatively small regions, where the stretching factors are much higher. During the optimization process, these regions converge more slowly and need special local optimizations.

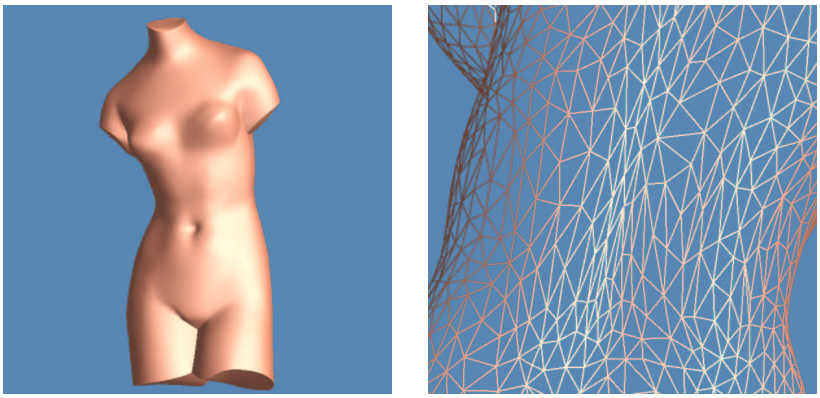

Venus Mesh Obtuse Angles

FIG. 5. *Negative String Constants*

The energy form $\sum k_{u,v}||f(u) - f(v)||^2$ is determined by $k_{u,v}$. During our experiments, we find that if $k_{u,v}$'s are all positive, then the algorithm converges faster and is more stable. Suppose there are two faces sharing an edge $[u, v]$ and α, β are the two angles in these faces opposite to the edge, then $k_{u,v}$ can be reformulated as

$$k_{u,v} = cot\angle\alpha + cot\angle\beta. \tag{50}$$

For the Venus model shown in figure 5, the barycentric embedding converges very fast. The harmonic optimization converges much more slowly. There are too many obtuse

angles on the triangle mesh, so many $k_{u,v}$'s are negative. In our implementation, we carry out some preprocessing on the meshes, to swap or split edges with negative $k_{u,v}$'s to convert their $k_{u,v}$'s to be positive. This process improves the convergence speed.

5. Applications. Global conformal structure has many applications in computational aided geometry design and graphics fields.

5.1. Computational Topology. While homology has a group structure, cohomology has a ring structure, so it can reveal more information of the manifolds. The cohomology bases can be used to detect the homology class of a closed curve. Suppose a cohomology basis $\{\omega_1, \omega_2, \cdots, \omega_{2g}\}$ has been computed, given an arbitrary closed curve r, if r is homologous to zero, then the following must hold

$$\int_r \omega_i = 0, \forall i. \tag{51}$$

If r is homologous to zero, we can find the domain whose boundry is r by the following simple flooding algorithm. First we label all the ajacent faces on the left of r. Then we label all of their neighboring faces on the left of them. We repeat this process until no further faces can be labeled. Then all the labeled faces form the desired domain.

5.2. Geometry Matching. Conformal structure is determined by Riemann metric, so it is independent of triangulation. Conformal structure is stable in the sense that if we perturbate the metric, the conformal structure changes continuously. Therefore, it is tolerant of noises and insensitive to different resolutions. We perform some numerical experiments to verify this property of conformal mappings. In figure 15 and 16, we have two different meshes representing the same geometry - a male face. One mesh has 5000 faces, the other one has 1000 faces. Both of them are conformally mapped to a unit disk with the same boundary condition and texture mapped with the same texture. By comparing figure 15 (c) with figure 16 (c), we can see the major geometric features are mapped to similar positions. On the contrary, the barycentric embedding heavily depends on triangulation and resolution, which is demonstrated by comparing figure 15 (b) and figure 16 (b).

Suppose we have two geometrically similar surfaces M_1, M_2, in order to find the best geometric match, we can conformally map them to a canonical domain D.

$$\begin{array}{ccc} M_1 & \xrightarrow{f_2^{-1}\circ f_1} & M_2 \\ & {\scriptstyle f_1}\searrow \quad \swarrow{\scriptstyle f_2} & \\ & D & \end{array} \tag{52}$$

Then $f_2^{-1} \circ f_1$ gives the desired geometric matching. In this process, the appropriate boundary conditions should be set up correctly. Figure 17 shows the geometric matching between two real human faces by conformal mapping. Figure 17(c) is the

original female face surface, (h) is the original male face surface. We first conformally map each of them to a unit square as shown in (a) and (b), then obtain the matching between them. In order to visualize the matching, we show the geometric morphing of the following homotopy:

$$t\ id + (1-t)\ f_2^{-1} \circ f_1,\ t \in [0,1]. \tag{53}$$

Although the geometries are quite different and the boundaries are not very similar, the result of the automatic matching process is quite satisfying as shown in figures 17 (c) to (h).

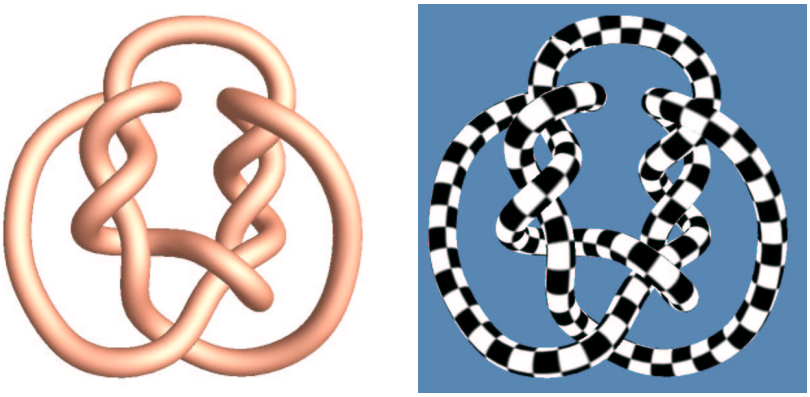

FIG. 6. *Knot mesh*

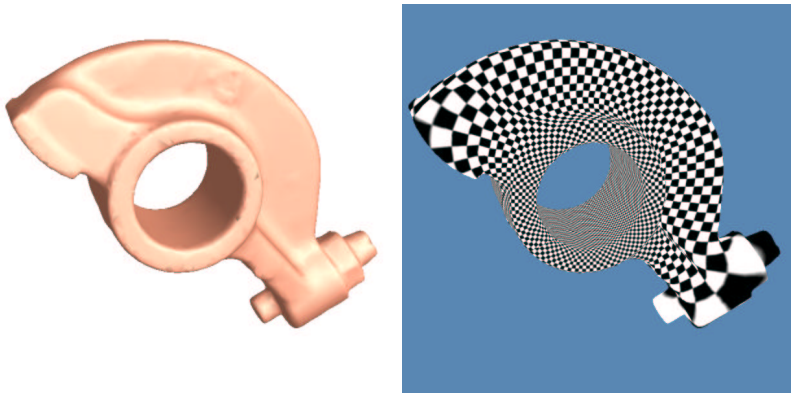

FIG. 7. *Machine Part*

5.3. Geometry Classification. The non-zero genus surfaces can be classified by their conformal structures naturally. After a basis of the holomorphic one-form group is computed, it is straightforward to compute the period matrices. During the construction of homology basis, we can obtain a canonical homology basis $\{e_1, e_2, \ldots, e_{2g}\}$, that is

$$e_i \cdot e_j = \delta_j^{i+g},\ i < j. \tag{54}$$

Then the *period matrix* is

$$\mathbf{P} = \begin{pmatrix} \int_{e_1}\zeta_1 & \int_{e_1}\zeta_2 & \cdots & \int_{e_1}\zeta_{2g-1} & \int_{e_1}\zeta_{2g} \\ \int_{e_2}\zeta_1 & \int_{e_2}\zeta_2 & \cdots & \int_{e_2}\zeta_{2g-1} & \int_{e_2}\zeta_{2g} \\ \cdots & \cdots & \cdots & \cdots & \cdots \\ \int_{e_{2g}}\zeta_1 & \int_{e_1}\zeta_2 & \cdots & \int_{e_{2g}}\zeta_{2g-1} & \int_{e_{2g}}\zeta_{2g} \end{pmatrix} = C + \sqrt{-1}S. \tag{55}$$

If two surfaces M_1, M_2 are conformally equivalent, then there exists an integral symplectic matrix N, such that $N^{-1}C_1^{-1}S_1N = C_2^{-1}S_2$ and $N^TC_1N = C_2$. N is the homology bases transformation matrix.

For the genus one case, the period matrix can be equivalently represented as *shape factors*. Each genus one surface can be conformaly mapped to a parallelogram. The shape factor is defined as length ratio of two adjacent edges and the acute angle of the parallelogram. The following are the shape factors of our computing results.

TABLE 1
Shape factors of genus one meshes

Mesh	Angle (degree)	Length Ratio	Figure	vertices	faces
Torus	89.9874	2.2916	Fig. 2	1089	2048
Teapot	89.95	3.0264	Fig. 3	17024	34048
Knot	85.1	31.150	Fig. 6	5808	11616
Machine Part	85.4321	4.9928	Fig. 7	3750	7500

General genus one meshes can be classified by shape factors and differentiated without resorting to further geometric features. The above results show that the knot mesh has the greatest length ratio, which meets our expectation. Teapot and Torus are symmetric, so the angles are right angles.

5.4. Global Conformal Parametrization. A mesh can be parameterized conformally by integrating holomorphic one-forms on it. The parametrization is globally conformal except for finite singularities. By changing holomorphic one-forms, the neighborhoods of singularities can be conformally parametrized too.

By using conformal parameters, many important geometric quantities which are valuable for geometric analysis can be computed explicitly. Figure 8 shows a level set of a special Morse function defined on the female face shown in figure 17 (c). The level set is displayed in (b) on the conformal parametrization domain and in (a) on the face surface. The singularities and Morse indices can be visualized directly. The configuration of these curves reveals rich information of the original geometry and offers a canonical way to decompose surfaces to patches.

6. Conclusion. This paper introduces a systematic way to compute conformal structures for general surfaces represented as triangle meshes. The homology is computed by simplicial complex structures. The dual cohomology basis is constructed

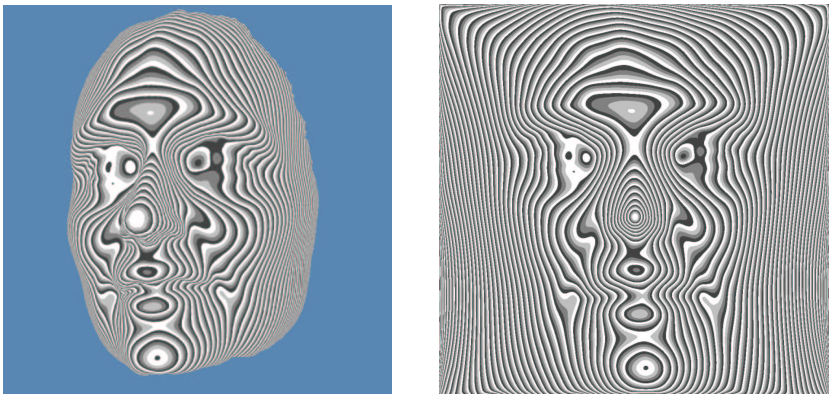

(a). level set on surface (b). Level set on parameter domain

FIG. 8. *Morse function Level set*

geometrically. Each cohomology cocyle is diffused to a harmonic one-form by adding an exact one-form. The Hodge star operation on the harmonic forms is formulated as a full rank sparse linear system. Then the basis of holomorphic differentials is constructed explicitly. To the best of our knowledge, this paper is the first one to solve this problem completely. The methods introduced here are very general. The harmonic one-forms, holomorphic one-forms have much broader applications. The conformal structure can be applied in many theoretic fields as well as engineering fields.

7. Future Research. Conformal structures of closed surfaces are studied thoroughly in this paper. We would like to generalize the results to open surfaces. The current computations are based on mesh structures. We will generalize the algorithms to other surface representations, such as implicit surfaces and level sets. The optimization of harmonic energy is computationally expensive. In the future, we will use multi-resolution methods to improve the speed. We will explore more on the relations between the eigenvalues, eigenfunctions of Laplace operator and geometry. The current conformal parametrization is unique up to the automorphism group of $H_1(M, \mathbb{Z})$. In a future paper, we will introduce a new method which is complete unique.

Acknowledgment. We gratefully thank Stanford University, Washington University, Georgia Institute of Technology and Cyberware for the models.

REFERENCES

[1] R. SILHOL, P. GIANNI, M. SEPPALA, AND B. TRAGER, *Riemann surfaces, plane algebraic curves and their period matrices*, Manuscript, 1996.

[2] M. SEPPALA, *Computation of period matrices of real algebraic curves*, Discrete Comput. Geom., 11(1994), pp. 65–81.

[3] P. BUSER AND M. SEPPALA, *Computing on Riemann surfaces*, Manuscript.

[4] K. Stephenson, *Approximation of conformal structure via circle packing*, Computational Methods and Function Theory, (1997), pp. 551–582.

[5] M. Eck, T. DeRose, T. Duchamp, H. Hoppe, M. Lounsbery, and W. Stuetzle, *Multiresolution analysis of arbitrary meshes*, In: Proceedings of ACM SIGGRAPH, Addison Wesley, Auguest 1995.

[6] S. Haker, S. Angenent, A. Tannenbaum, R. Kikinis, G. Sapiro, and M. Halle, *Conformal surface parameterization for texture mapping*, IEEE Transactions on Visualization and Computer Graphics, 6(2000), pp. 240–251.

[7] M. Meyer, P. Alliez, and M. Desbrun, *Interactive geomety remeshing*, In: Proceedings of ACM SIGGRAPH, Addison Wesley, 2002.

[8] N. Ray, B. Levy, S. Petitjean, and J. Maillot, *Least squares conformal maps for automatic texture atlas generation*, In: Proceedings of ACM SIGGRAPH, Addison Wesley, 2002.

[9] R. Schoen and S. T. Yau, *Lectures on Harmonic Maps*, International Press, Harvard University, Cambridge MA, 1997.

[10] A. Derose, T. Duchamp, A. Certian, and W. Stuetzle, *Hierarchical computation of pl harmonic embeddings*, preprint, July 1997.

[11] E. Arbarello, M. Cornalba, P. Griffiths, and J. Harris, *Topics in the Theory of Algebraic Curves*, 1938.

[12] Weyl H, *On generalized Riemann surfaces*, Ann. of Math., 35(1934), pp. 714–729.

[13] C. L. Siegel, *Algebras of Riemann Matrices - Tata Institute of Fundamental Research*, Lecture on Mathematics and Physics, Tate Institute Bombay, 1956.

[14] J. R. Munkres, *Elements of Algebraic Topology*, Addison-Wesley Co., 1984.

[15] H. Hoppe, *Progressive meshes*, In: Proceedings of ACM SIGGRAPH, pp. 99–108, Addison Wesley, 1996.

[16] X. Gu, S. J. Gortler, and H. Hoppe, *Geometry images*, In: Proceedings of ACM SIGGRAPH, Addison Wesley, 2002.

[17] M. S. Floater, *Parametrization and smooth approximation of surface triangulations*, Comp. Aided Geom. Design, (1997), pp. 231–250.

(a). Gargoyle mesh (20000 faces)

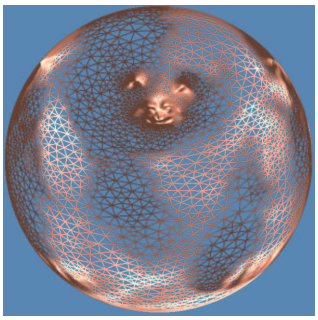

(b). Barycentric mapping

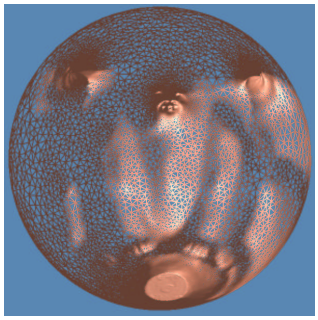

(c). Conformal map of gargoyle

(d). Conformal texture-mapping

FIG. 9. *Spherical Barycentric Mapping for gargoyle model*

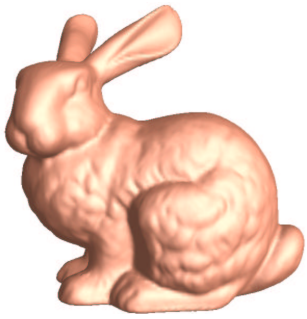

(a). Bunny mesh (20000 faces)

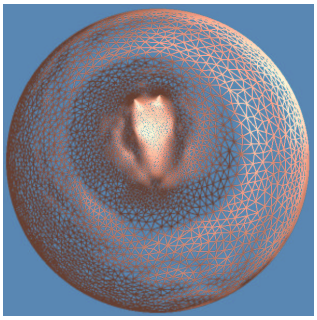

(b). Conformal map of Bunny

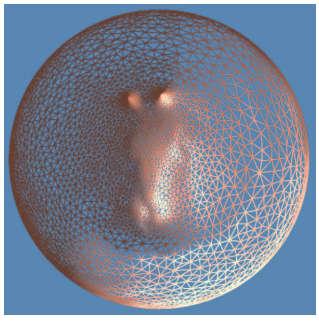

(c). Mobius transform of (b)

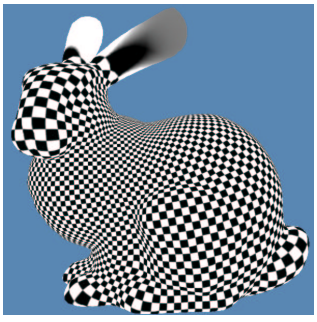

(c). Conformal texture-mapping

FIG. 10. *Spherical conformal maps of the bunny meshes*

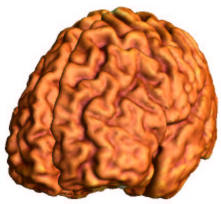

(a). Brain mesh (20000 faces)

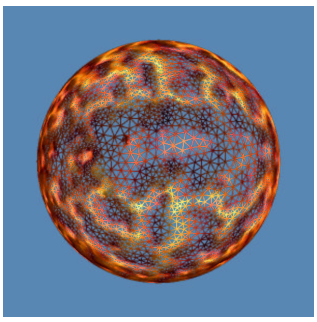

(b). Spherical barycentric mapping

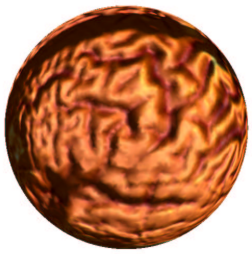

(c). Conformal map of brain

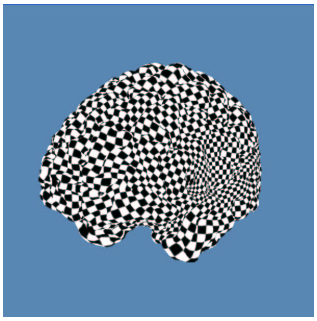

(d). Conformal texture-mapping

FIG. 11. *Spherical conformal mapping of the brain mesh*

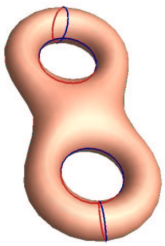

(a). Homology bases

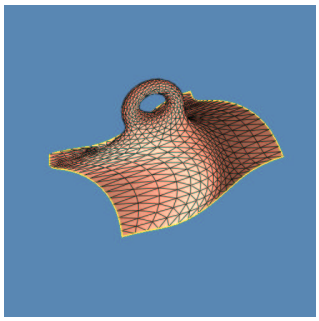

(b). Open one handle

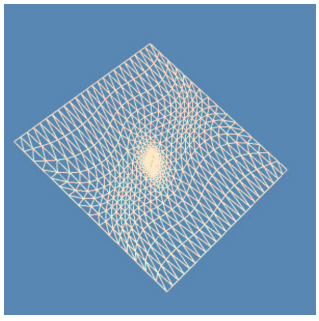

(c). Map to square

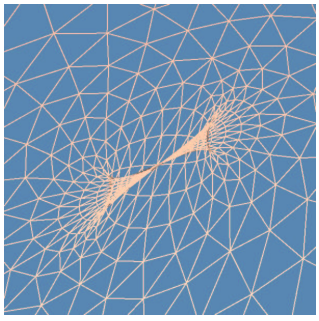

(d). Zoom in to central region

FIG. 12. *Computing Homology and Cohomology*

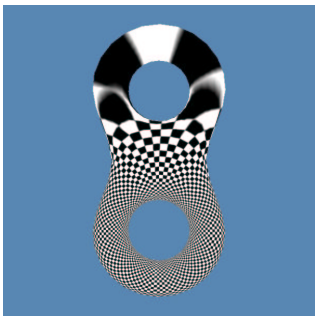

(a). Holomorphic one-form ζ_1

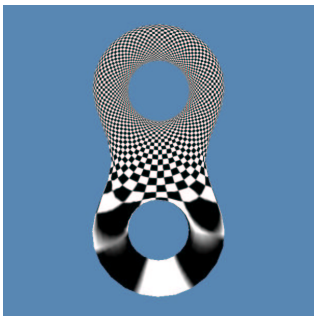

(b). Holomorphic one-form ζ_2

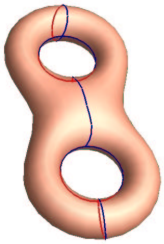

(c). Boundary on mesh

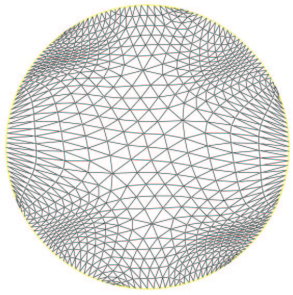

(d). Fundamental domain

FIG. 13. *Bases of Holomorphic differentials*

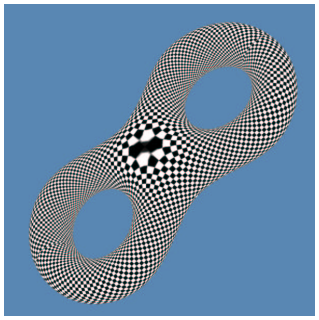

(a). $\zeta_1 + \zeta_2$

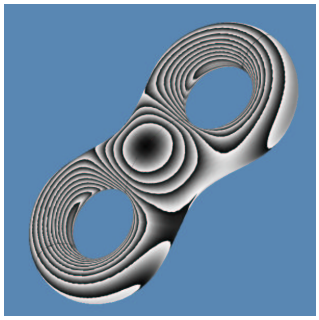

(b). Streching factor level sets

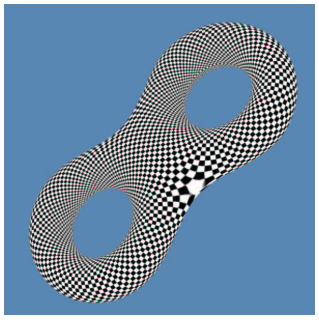

(c). $\zeta_1 - \zeta_2$

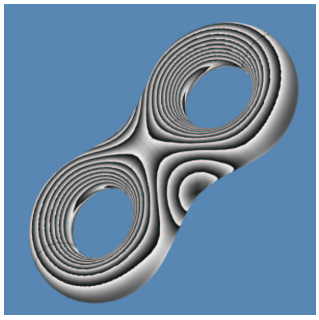

(d). Streching factor level sets

FIG. 14. *Holomorphic one-form and level sets of streching factor*

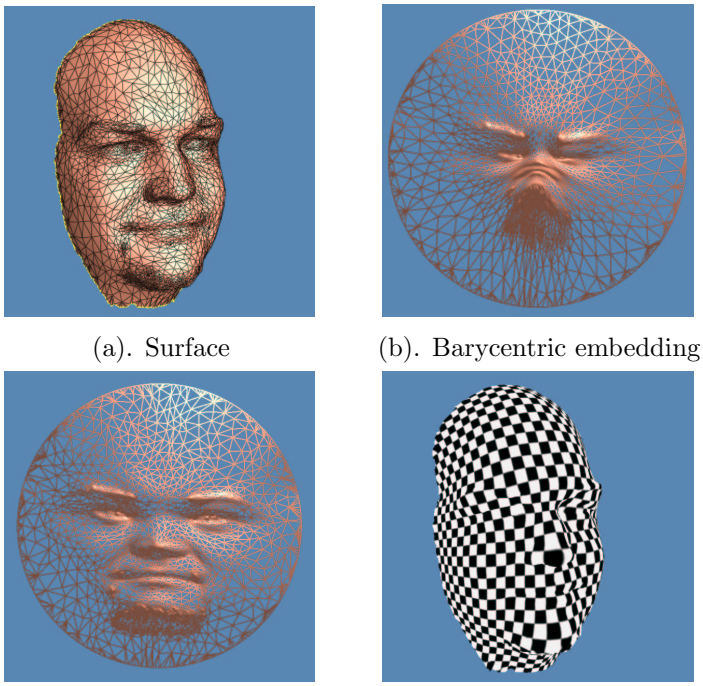

(a). Surface (b). Barycentric embedding

(c). Conformal embedding (d). Conformal texture-mapping

FIG. 15. *Male face surface with 5000 faces*

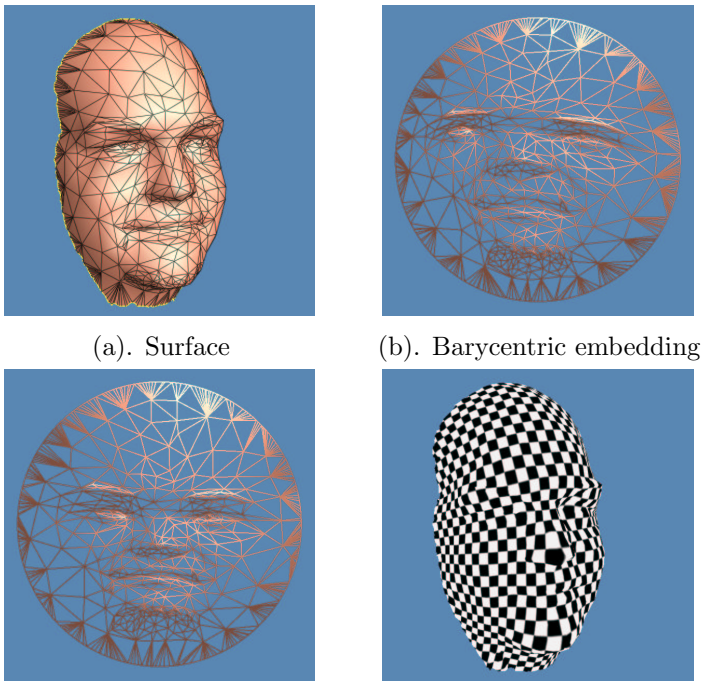

(a). Surface (b). Barycentric embedding

(c). Conformal embedding (d). Conformal texture-mapping

FIG. 16. *Male face surface with 1000 faces*

(a). Female parametrization

(b). Male Parametrization

(c). t = 0.0

(d). t=0.2

(e). t = 0.4

(f). t = 0.6

(g). t= 0.8

(h). t= 1.0

FIG. 17. *Geometric matching by conformal parametrization*